# Direct Metal Laser Fabrication of Cu slabs from powder precursor: surface depth of melt and furnace temperature issues

Jorge Ramos-Grez[1], Jorge Sanz-Guerrero, Tomás Larraín, Andrés Ramírez

Mechanical and Metallurgical Engineering Department
Pontificia Universidad Católica de Chile
Av. Vicuña Mackenna 4860 – Macul – Santiago - CHILE

## ABSTRACT

A DMLF processing unit based on a raster-scanned 80 W $CO_2$ laser beam has been developed to process single layers of metallic powder precursor. The process chamber provides atmosphere control (high vacuum and inert gas refill) besides temperature elevation up to 700 $^{o}$C. In this work, copper powder precursor is confined inside a refractory steel mask surrounded by an aluminum oxide jacket that acts as insulator. The powder layers can have thicknesses of 0,5 and 1 mm. An infrared pyrometer measures in real time the temperature at one location in the surface of the powder bed. Scan speed, scan step, and furnace temperature have been varied to find combinations of such parameters that render surface melting and maximum densification. Partially melted samples were produced and their mass density was measured. Micro-hardness and surface roughness were also measured along the resolidified surface, the first rendering an average of 80,6 HV compared to the 90-105 HV of oxygen free copper, while the second resulting in an 8 μm $R_a$ value. Maximum melt of depth achieved is ~0,15 mm followed by a sintered layer.

## INTRODUCTION

The "Direct Metal Laser Fabrication" (DMLF) process was developed at the end of the 90s by the inventors of the "Selective Laser Sintering" (SLS™), which was patented and commercialized previously and successfully at the beginning of the same decade (Deckard 1989 [1] and Beaman *et al* 1997 [2]). The SLS™ process has allowed making a major step in the fabrication of complex geometry prototypes from polymers in freeform. This has also allowed shortening the design and fabrication cycle of high added value products. On the other hand, the DMLF process was developed afterwards with the objective to process metals in freeform directly, to recover high added value mechanical components (e.g., turbine blades) as well as obtain functional prototypes of complex geometry, this is, could withstand high temperatures and high mechanical stresses (Das *et al* 1998 [3]). Need for a rapid manufacturing of metal molds and dies was another reason that pushed the development towards this type of technology (Atwood *et al* 1998 [4]; Lü *et al* 2001 [5]). However, it has to be mentioned that the DMLF process is one that still finds itself at a experimental phase and only the indirect-Selective-Laser-Sintering (iSLS, 3DSystems EEUU), Direct-Metal-Laser-Sintering (DMLS, EOS Germany) and Laser-Engineering-Net-Shaping (LENS, Optomec EEUU) have been commercialized in past years. Recent publications verified this argument (Venuvinod y Ma 2004 [6]; Erzincanh and Ermurat 2005 [7], Simchi *et al* 2003 [8,9]; Tang *et al* 2003 [10]; Zhu *et al* 2003

[1] Corresponding author: jramos@ing.puc.cl

[11,12]; Morgan *et al* 2004 [13]; Ning *et al* 2006 [14]). Among the main problems not been yet solved, we find: a resulting high superficial roughness of the component made this way (*i.e.,* > 16 μm), presence of porosity and in certain cases a lack of densification (less that a 100%), and residual stresses (Nickel *et al* 1999 [15]). Oxygen and nitrogen contamination is yet another important issue that has to be considered, too.

Most common metallic alloys used with the DMLF technology are those of Ti-Al-V (Wu and Mei 2003 [16]), Cu-$Cu_3P$ (Tang *et al* 2003 [10], Zhu *et al* 2003 [11, 12]), Fe-C-Cu-Mo-Ni (Simchi *et al* 2003 [8,9]) and Cu-SCuP (Ning *et al* 2006 [14]) among others. During 2003, Kyogoku *et al* [17] did preliminary trials using DMLF to process a Ti-Ni alloy. In this opportunity, Kyogoku *et al* showed the feasibility to produce polycrystalline structures with cylindrical shape (25 mm in length x 2-3 mm in diameter) by means of DMLF from a equi-atomic alloy composition of Ti and Ni. These components showed the shape memory effect when analyzed by differential scanning calorimetry.

During 2003, Ramos *et al* [18] carried out preliminary trial of DMLF at the University of Texas at Austin using Cu powder precursor. In that occasion, Cu specimens were obtained with the acceptable surface integrity. The grain size obtained varied from 10 to 100 μm in average transversal diameter. Longitudinally the grains showed a dendritic columnar morphology that was oriented towards the thermal gradient caused by the motion of the heat source. In this opportunity, room temperature conditions were kept at the interior of the processing chamber and a 240 W power laser was used at a wavelength of 1,06 μm. The latter power level was enough to achieve complete melting of the pre-placed powder layer; moreover, at such wavelength enhanced coupling of the laser beam into the material takes place.

## THEORETICAL FRAME WORK

The Direct Metal Laser Fabricación (DMLF) process

In the DMLF process, bonding of metal powder particles (*i.e.*, 10 to 50 μm in diameter) is achieved by means of pressureless sintering at high temperatures and in other situations by the partial or total melting of a layer of powder rendering a liquid phase sintering process. In both cases, a high power infrared laser beam is used. The laser is raster scanned by means of an oscillating mirror system. The laser beam interacts over the surface of the powder layer, which has been previously compacted to thickness of 0,1 mm to 0,5 mm. This layer is previously heated to a temperature in between 0,6 to 0,8 of the melting temperature of the powder, which is immerse inside an inert and reducing atmosphere (*e.g.,* Ar-$H_2$). The energy provided by the laser beam increases the temperature locally over the temperature at which sintering or melting take place (Beaman *et al* 1997 [1]). In this way, a bidimensional solid slab (solid layer) of low thickness is made.

Reduction in the surface area of the powder is another driving force for the densification at ambient pressure (Bourell *et al* 2002 [19]; German 1984 [20]). Once a dense layer of material is fabricated this way, the process can be repeated many times rendering a multi-layered volumetric object as final result. The powder that surrounds the part and that has not been sintered or melted is afterwards removed manually. Among several other investigators, Zhu *et al* (2003) [21] have implemented a multi-layer DMLF process.

If the process is carried out using a single layer of compacted powder but of greater thickness (typically 1 mm to 4 mm), the result will also be a solid slab or rod with high degree of densification. However, under this configuration a phenomenon called "balling" takes place when the quantity of melted material surpasses a critical level, together with the effect of a surface tension gradient in the liquid and with the magnitude of the enthalpy of reaction between the liquid and the atmosphere above it. All these factors can induced surface ripples, and in some cases spherical agglomerates (Anthony and Cline 1977 [22]; Ramos 2003 [23]; Rombouts *et al* 2005 [24]). By controlling the process parameters, it is possible, even for large layer thicknesses, to achieve acceptable cylindrical geometries 2-3 mm in diameter (Kyogoku *et al* 2003 [17]). Figure 1 show the schematic of the experimental apparatus used by Ramos and Kyogoku to achieve the single layer DMLF process of a shape memory alloy (Ti-50.2at%Ni).

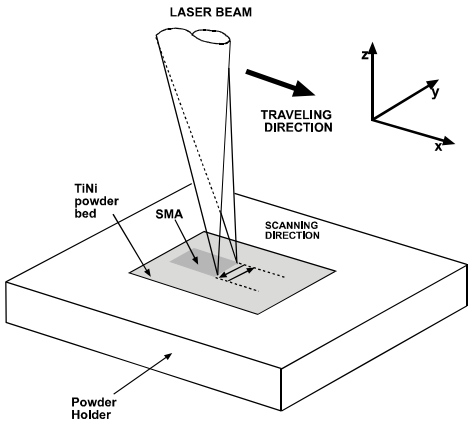


Figure 1. Schematic of the DMLF process for single powder layer (Ramos 2003 [23])**.**

Process parameters

When a scanning mirror system is used to modulate the laser beam over the powder layer, energy can be deposited spatially. This determines the temperature gradient that operates over the powder layer, determining the degree of sintering between layers or the fraction of melted material. Solidification of melted material is a function of the thermal gradient and the speed of the solidification front is related to the scanning speed of the laser beam. Time modulation of the laser beam during the melting regime also plays a critical role in densification of the resulting solid (Morgan *et al* 2004 [13]), however in this research this variable was not considered.

Finally, it has to be mentioned that the large melting point of Cu, it affinity to become contaminated with oxygen and surface tension fluctuation in the liquid phase make this process very complex to control. Due to the fact that the powder layer temperature can reach above 800 ºC, it is necessary to operate under vacuum conditions (*i.e.*, higher than $10^{-2}$ torr) and then refill the furnace chamber with a reducing-inert gas to avoid residual oxygen contamination of the powders (Das *et al* 1998 [3]; Ramos 2003 [23]). To avoid grain growth in the specimens, due to the high temperatures at which the vacuum furnace is set, once the laser beam has been scanned, inert gas can be used to purge the atmosphere inside the furnace to further cool down the alloy fast enough to avoid structural transformation to take place. A virtual representation of the DMLF system developed and used in the present work is shown in Figure 2.

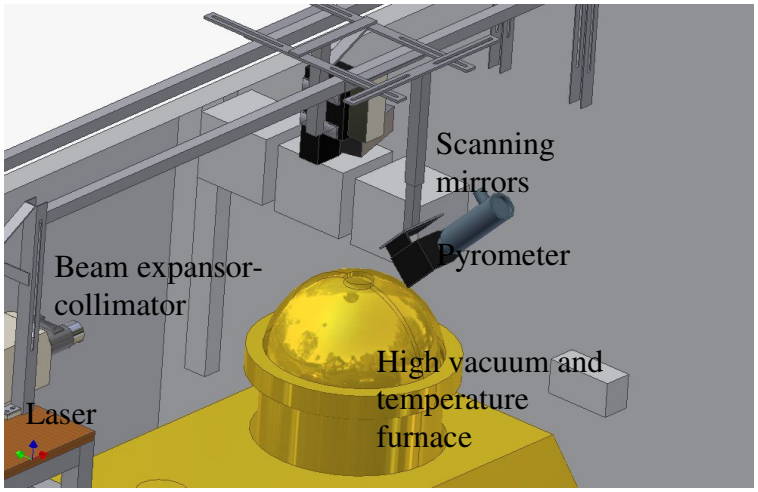


Figure 2. Virtual design of the available equipment to perform the Direct Metal Laser Fabrication process.

Hypothesis

The main hypothesis of the present work considered the feasibility to obtain surface melting and sintering of a powder bed of Cu powder by the DMLF process using a low power laser beam (80 W) if the right processing parameters combination is found: laser scan speed, percentage beam overlap and furnace temperature. A secondary hypothesis that evolved, is that at low laser power, initial temperature of the powder bed (i.e., temperature inside the furnace) beyond a certain value for a given powder precursor could hinder melt formation.

## EXPERIMENTAL SET UP

In July 2004 Ramos *et al*, started to develop a capacity to fabricate Cu alloys using the Direct-Metal-Laser-Fabrication (DMLF) technology with fundings form Fundación Andes in Chile. This project contemplated setting up a system to do the DMLF process, integrating several subcomponents previously available as well as acquired with the funding available from that project (Figure 3). In this system, focusing is done using a F-theta lens with 36 cm of focal length resulting in a focusing diameter of 0,296 mm. Motion of the laser beam is achieved by a pair of scanning mirrors. Vacuum level and temperature inside the furnace are also operating up to $10^{-3}$ Torr and 700 °C, respectively. Figure 4, shows the pair of scanning mirrors located over the furnace window and the infrared pyrometer, which can measure surface temperature at one fixed location inside of the furnace. At present, the pyrometer is used to measure and control temperature at one fixed position by a PI closed loop scheme that actuates on the laser power intensity. The control systems behaves according to the following transfer function,

$$G(s) = \frac{K_G \cdot e^{-0,1s}}{1 + 0,8s}. \qquad (1)$$

The static gain, $K_G$, has been determined empirically for a temperature range measured between 450°C to 900 °C at the surface of the copper powder, and its behavior is shown in Figure 5. It suggests that the heat source is no linear with respect to the gain and the percentage of power delivered. Nonetheless an average value of $K_G$ of 97,94454 was taken as a good approximation.

Figure 3. DMLF system showing $CO_2$ laser unit 80 W SYNRAD, an Edwards vacuum and temperature furnace, Cambridge Technology galvanometric mirrors.

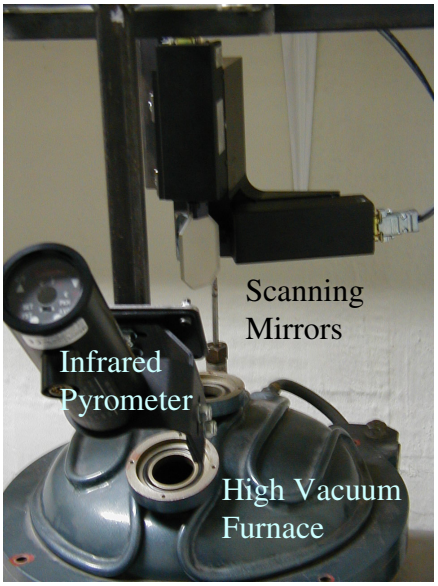


Figure 4. System components of the DMLF machine: high vacuum and temperature furnace, infrared pyrometer and scanning mirrors.

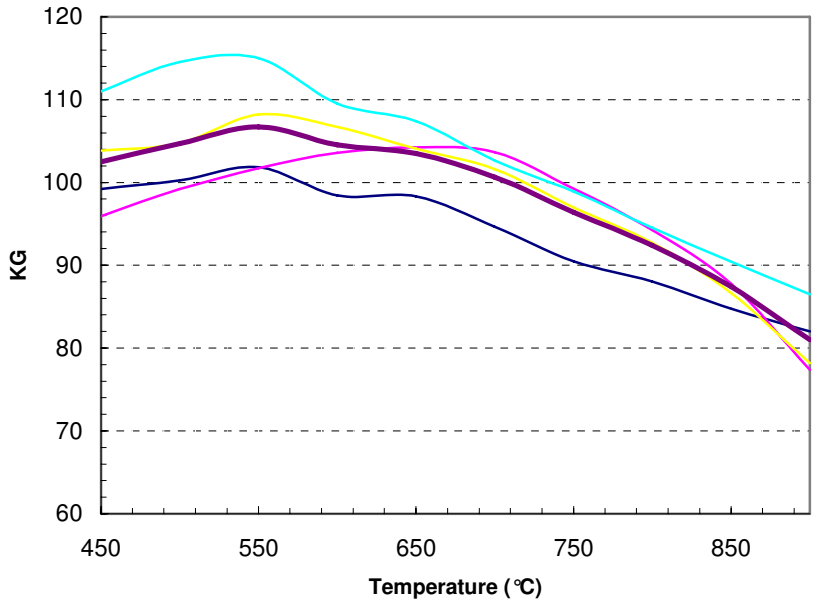


Figure 5. Plot of the static gain $K_G$ of the temperature control system for different set parameters.

It convenient to mention that the available $CO_2$ laser unit was used at a maximum power level of 80 W before reaching the scanning mirrors, which translates into a 55+/-5 W power at the powder surface with a wavelength of 10,6 µm. This lack of laser power, narrows the experimentation range (leaving off materials systems with melting points above 1100 °C), so that in current research, laser power was kept at a maximum level. Moreover, the laser beam can perform a zig-zag or "snake" scanning pattern to simulate a linear heat source, as shown in Figure 6.

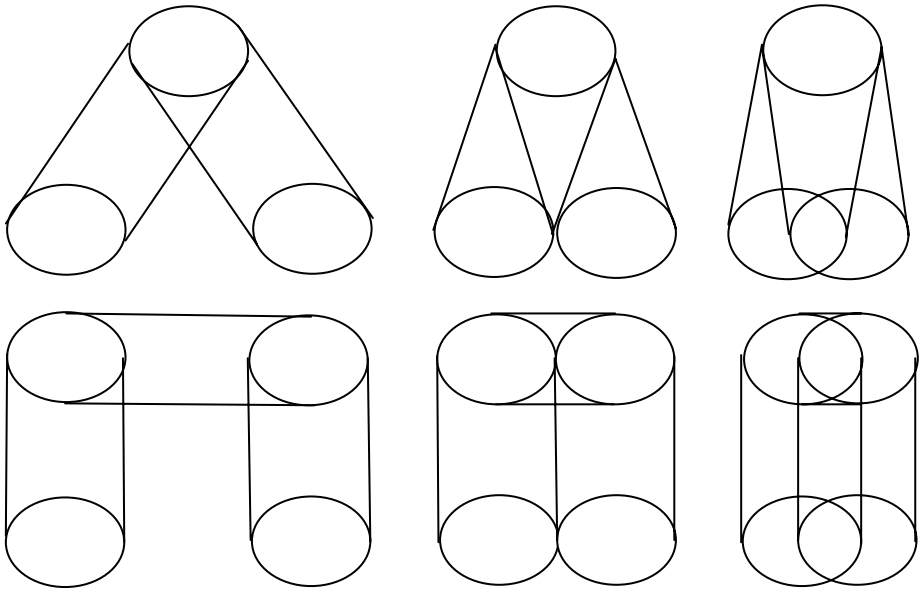

Figure 6. Laser beam raster scan patterns: zig-zag (up) and "snake" (down) type, showing different levels of beam overlap increasing from left to right.

High temperature inside of the process chamber is achieved by an array of up to 6 loops of Kanthal™ wire heating elements (2 to 3 mm in diameter) by a mechanism of heat radiation when passing a current of up to 75 amperes at a voltage of 18 volts (Figure 7). Maximum temperature achieved is 710 °C. The powder steel holder is located inside the volume surrounded by the heating element array. It consists of a refractory steel mask having a 0,5 mm and 1,0 mm deep troughs and is surrounded by an aluminum oxide insulating jacket, as illustrated in Figure 8.

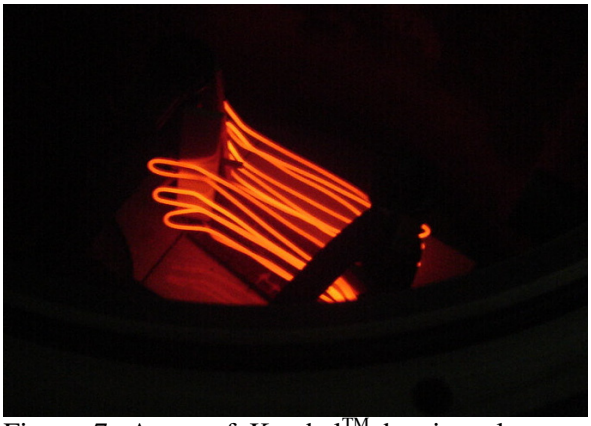

Figure 7. Array of Kanthal™ heating elements glowing inside of the processing chamber.

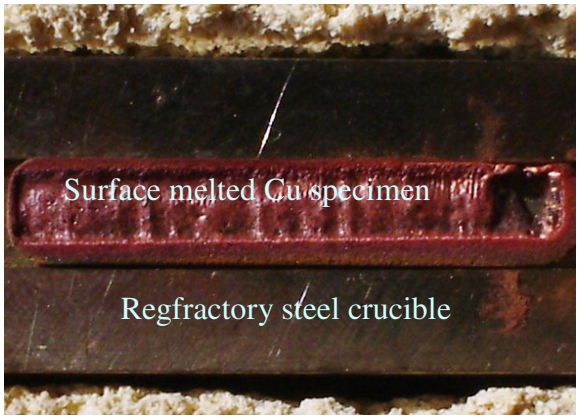


Figure 8. Refractory steel mask and insulating alumina jacket used to hold the pre-placed Cu powder during the DMLF which has already been melted.

## EXPERIMENTAL TECHNIQUES

Specimen fabrication

The copper powder precursor was preplaced inside the trough of the refractory steel mask, which was then inserted in the porous alumina enclosure. Masks had two different trough depths, 0,5 mm and 1 mm. The powder holder was then located inside of the processing chamber at the heating elements zone. The chamber is closed and

clamped and a mechanical pump draws vacuum up to 300 mTorr pressure. A coiled tube surrounds the chamber acting as a cooling water jacket. The chamber is then filled with argon gas, purged and then filled back again. The furnace heating elements are energized by increasing the amperage slowly up to 70 amps. This heating procedure takes ~20 minutes and then the laser beam is turned on to an 80 watts power level. The laser beam is expanded 8 times its size and collimated using a telescope, being then modulated in space by a pair of scanning mirrors. These reflect the beam downwards trough the F-theta lens which focuses it inside the chamber at the surface of the powder bed. The laser beam enters the chamber trough a ZnSe window. Two process variations where considered, tuning off the furnace heating elements just before the laser beam started to scan and turning it off right after it finished scanning. Once the fabrication is accomplished, the specimens were allowed to cool down slowly for two hours until a temperature of 30 °C was reached inside the chamber.

Characterization techniques

An analytical weighting machine with four digit precision was used to weight the resulting specimens. Mass density was calculated by carefully measuring the dimension of the specimens by means of a micrometer to compute the volume. The infrared pyrometer was used to sample the temperature of the powder surface at one specific and fixed point (middle point of specimen width). A contact surface profile meter was used to measure arithmetic surface roughness of the specimens that experience melting, and a micro hardness Vickers tester was used to measure the surface micro hardness of those specimens, too.

## RESULTS AND DISCUSSION

The characterization of the powder precursors as well as of the resulting specimens was done. Temperature histories at one fixed location in the powder bed surface were also measured. Results are presented as follows.

Characterization of the Cu powder precursor

The morphology of the Cu powder particles is shown in Figures 9 and 10 at different magnifications. Particle size ranged from 10 to 50 μm in diameter. These are not spherical particles but amorphous in shape. EDS chemical analysis was done on the powder to determine the presence of oxygen and other impurities content. From Figure 11 presence of oxygen is negligible and the small aluminum peaks corresponds to the sample holder.

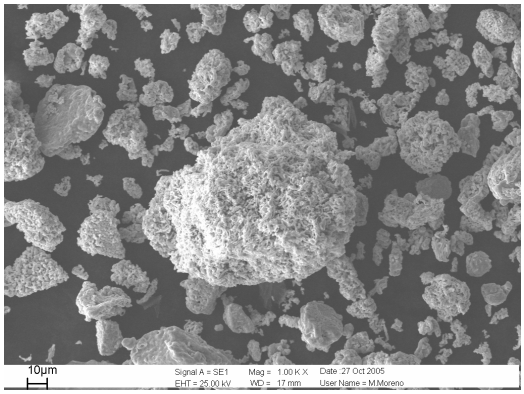


Figure 9. Cu powder precursor SEM characterization, 1000x.

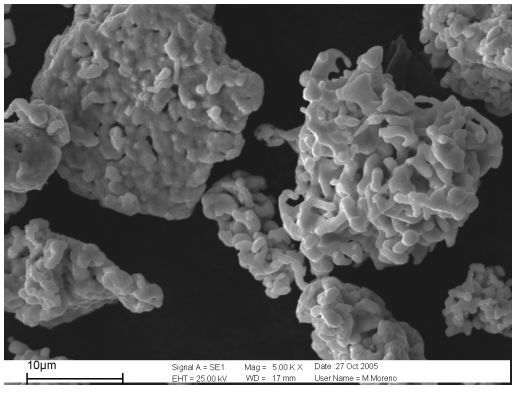


Figure 10. Cu powder precursor SEM characterization, 5000x.

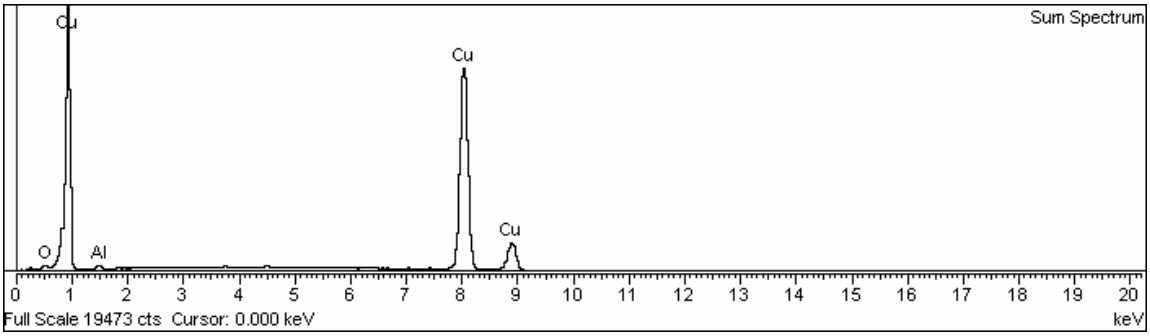

Figure 11. EDS chemical analysis of the Cu powder used as precursor.

Characterization of the laser processed Cu specimens

A total of 18 specimens were fabricated, of which only 7 underwent melting at the surface of the sintered powder body. The parameters used to fabricate these specimens are listed in Table 1. All of the specimens where made with a laser power fixed of 70% it maximum capacity, approximately 66 watts before the F-theta lens. Figures 12 to 18 show macro pictures of the surface of all the specimens that melted. Figure 19 shows a macro picture of Specimen #18, which did not undergo complete melting at the surface but instead liquid phase sintering. This specimen was however, fabricated under the highest average furnace temperature, almost 65°C more than Specimen #17. Another difference between these two specimens is that the latter was processed at a traverse speed twelve times faster.

Table 1 Summary of processing parameters used in specimens that achieved surface melting (except for Specimen #18). Vs: scanning speed, ss: scan step, BOL: beam overlap, Vt: traverse speed, P: laser power, Tavg: average furnace temperature

| # | Vs (mm/s) | ss (mm) | BOL % | Vt (mm/s) | P/Vt (J/mm) | P/Vs (J/mm) | Tavg (°C) | Scan time (s) |
|---|---|---|---|---|---|---|---|---|
| 3 | 20,1 | 0,1500 | 48 | 0,94 | 70,3 | 3,3 | 499 | 32 |
| 4 | 19,3 | 0,1500 | 48 | 0,94 | 73,5 | 3,4 | 480 | 33 |
| 5 | 20,0 | 0,1500 | 48 | 0,94 | 70,3 | 3,3 | 498 | 32 |
| 6 | 19,0 | 0,1500 | 48 | 0,89 | 74,5 | 3,5 | NA | 34 |
| 7 | 19,0 | 0,1500 | 48 | 0,89 | 74,5 | 3,5 | 498 | 33 |
| 12 | 23,7 | 0,1258 | 57 | 0,92 | 71,5 | 2,8 | 568 | 22 |
| 17 | 17,8 | 0,1500 | 48 | 1,22 | 54,2 | 3,7 | 660 | 25 |
| 18 | 13,4 | 0,0148 | 95 | 0,10 | 661,0 | 4,9 | 720 | 205 |

Figures 13 and 15 show that the powder bed layer thickness of 0,5 mm in Specimens # 4 and # 6 was too small and during melting, loose powder was dragged into de fusion zone depleting other areas from material, resulting in empty regions. Figures 12, 16, 17 and 18 illustrate that for a 1 mm layer thickness, homogenously melted surfaces were obtained for Specimens # 3, # 7, # 12 and # 17 all along the length of the powder bed. The crater observed at the left side on each of these images, is due to the stationary position of the laser beam at the start of the fabrication and to the delay to reach its operating power level. Specimen #5 shown in Figure 14 was fabricated with a layer thickness of 6 mm contained in a ceramic crucible, surface melting was also homogeneously achieved, probably because the ceramic crucible retains heat more efficiently than the metal mask.

Finally, from Figure 19, it can be seen that the surface of the Specimen # 18 has only melted partially favoring liquid sintering. One hypothesis as to why it did not melted

completely, even though it experienced the highest average furnace temperature (725 °C) and the longer laser material interaction time (eight fold greater), is the fact that surface heat losses by radiation could have surpassed the heat input from the laser beam coupling. Heat losses by radiation heat transfer increase with the fourth power of the surface temperature according to Stefan Boltzmann´s Law. Moreover, the applied laser power in this process was not high (~55 W at the surface of the powder bed). Finally, according to Ujihara (1972) [25], reflectivity of metals is shown to decrease with increasing surface temperature, thus discarding the possibility of a surface reflectivity increase in the infrared region with increasing temperature.

Figure 12. Specimen #3, laser power 66 W, Vs 20,1 mm/s, beam overlap 48%, Vt 0,94 mm/s, $T_{avg}$ 499 °C, scan time 32 s. Layer thickness 1 mm.

Figure 13. Specimen #4, laser power 66 W, Vs 19,3 mm/s, beam overlap 48%, Vt 0,94 mm/s, $T_{avg}$ 480 °C; scan time 33 s. Layer thickness 0,5 mm.

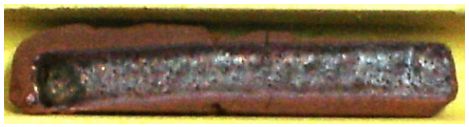

Figure 14. Specimen #5, laser power 66 W, Vs 20 mm/s, beam overlap 48%, Vt 0,89 mm/s, $T_{avg}$ 498 °C, scan time 32 s. Layer thickness 6 mm.

Figure 15. Specimen #6, laser power 66 W, Vs 19 mm/s; beam overlap 48%, Vt 0,88 mm/s; scan time 34 s. Layer thickness 0,5 mm.

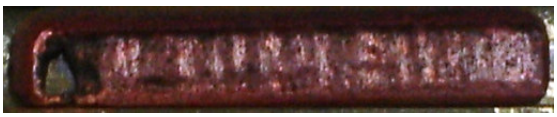

Figure 16. Specimen #7, laser power 66 W, Vs 19 mm/s, beam overlap 48%, Vt 0,89 mm/s, $T_{avg}$ 498°C, scan time 33 s. Layer thickness 1 mm.

Figure 17. Specimen #12, laser power 66 W, Vs 22,7 mm/s, beam overlap 57%, Vt 0,92 mm/s, $T_{avg}$ 568 °C, scan time 22 s. Layer thickness 1 mm.

Figure 18. Specimen #17, laser power 66 W, Vs 17,8 mm/s, beam overlap 48%, Vt 1,2 mm/s, $T_{avg}$ 660 °C, scan time 25 s. Layer thickness 1 mm.

Figure 19. Specimen #18, laser power 66 W, Vs 13,4 mm/s, beam overlap 95%, Vt 0,1 mm/s, $T_{avg}$ 720 °C, scan time 205 s. Layer thickness 1 mm.

Concerning the micro hardness Vickers measurements done on the specimens that showed complete surface melting, it can be seen in Table 2 that a value between 70 HV to 87 HV was recorded, which is lower when compared to the nominal hardness of an oxygen free copper sheet (90 to 105 HV [26]). Except for Specimen # 12, there is a trend between the measured mass density and the micro hardness HV at the surface of the specimens that melted as illustrated in Figure 20. On the other hand, the width W of the specimens can be twice as large as the scan pattern width programmed. The surface arithmetic roughness ($R_a$) measured resulted near to 8 μm, which is lower than values reported in literature.

**Table #2 Surface micro hardness Vickers, mass density and arithmetic surface roughness of specimens that experienced surface melting**

| # | A1 | A2 | A | B1 | B2 | B | C1 | C2 | C | Average HV | ρ (kg/m$^3$) | W (mm) | Ra (μm) |
|---|---|---|---|---|---|---|---|---|---|---|---|---|---|
| 3 | 88 | 75 | 82 | 89 | 86 | 88 | 79 | 83 | 81 | 83 | 3083 | 3,45 | NA |
| 5 | 107 | 82 | 95 | 93 | 57 | 75 | 62 | 79 | 71 | 80 | 2467 | 4,4 | NA |
| 7 | 91 | 76 | 84 | 112 | 78 | 95 | 70 | 93 | 82 | 87 | 3348 | 4,4 | 8 |
| 12 | 93 | 68 | 81 | 64 | 63 | 64 | 76 | 57 | 67 | 70 | 3539 | 4 | 8 |
| 17 | 68 | 83 | 76 | 84 | 116 | 100 | 90 | 56 | 73 | 83 | 3073 | 3,5 | 8 |

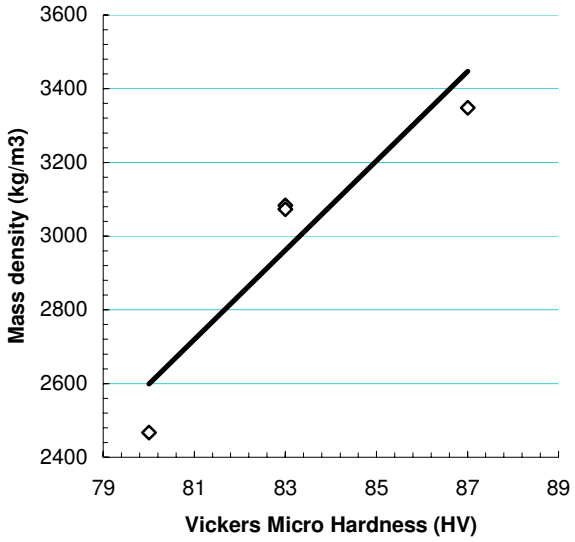


Figure 20 Plot of the mass density versus Vickers micro hardness of Specimens # 3, # 5, # 7 and # 17, showing a linear trend.

Finally, Figures 21 to 24 shows several macro pictures of Specimen # 12. The melted and resolidified surface shows a rippling pattern which could be due to surface tension gradients which tend to form surface waves that could freeze before their amplitude is completely dumped, moreover, pulling loose power into the melt front from the peripheral zones. The depth of melt in this specimen is ~0,15 mm followed by a sintered layer.

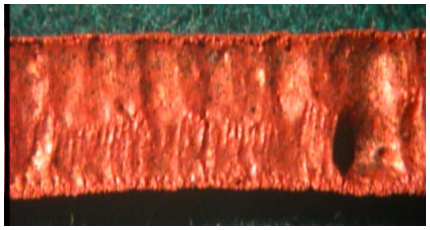

Figure 21. Specimen # 12, melted front surface indicating rippling.

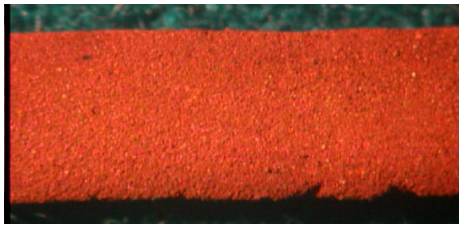

Figure 22. Specimen # 12, sintered back surface.

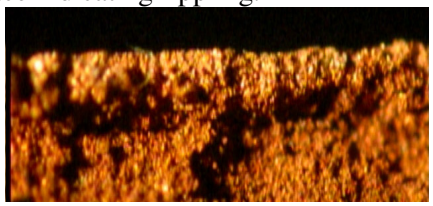

Figure 23 Specimen # 12, cross section indicating that the melted surface layer has a depth of 0,15 mm.

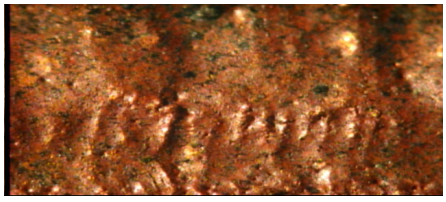

Figure 24 Specimen # 12, closed up pf melted front surface indicating frozen surface waves.

Furnace temperature issues

All specimens up to # 12 where fabricated so that the furnace heating elements were turned off when the laser beam started to scan over the powder bed surface. For the remaining specimens, the furnace was turned off only after the laser beam had completely scanned the surface of the powder bed. Figure 25 shows a plot of depth of melt versus furnace temperature, resulting from a simplified lumped heat balance model (Equation 2), that includes heat losses by radiation (including similar process parameters and constant temperature properties of copper taken from ref. 27 and $\varepsilon = 0{,}9$; $\eta = 0{,}1$; W = 3 mm; A = 15 mm x W). From this plot, it can be noticed that beyond a critical surface temperature (or equivalently furnace temperature, $T_0$) of 700°C, before the laser beam heats the surface spot, the depth of melt $d_m$ achieved reduces as the furnace temperature increases.

$$d_m(T_0) \simeq \frac{P \cdot \eta - A \cdot \varepsilon \cdot \sigma \cdot T_0^4}{v_t \cdot W \cdot \rho \cdot C_p (T_m - T_0)} \qquad (2)$$

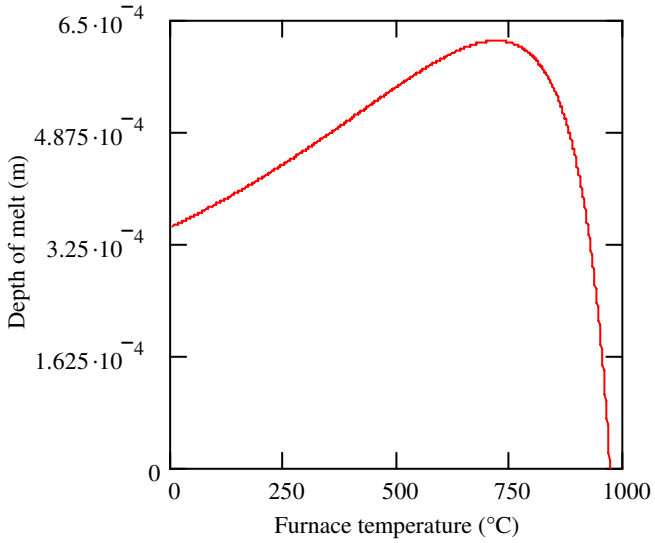


Figure 25 Depth of melt from the surface of the powder bed as function of the furnace temperature for a low power laser beam impinging on the surface.

This result is counter intuitive, however, surface temperature measurements of Specimens # 17 and # 18 validate this result. In the first plot, Figure 26, the change in temperature that takes places when the laser beam traverses the fixed spot, as measured by the pyrometer, is approximately 200 °C, for an average furnace temperature of 660°C. On the other hand, Figure 27 shows that an increase in temperature of the order of only 120 °C has taken place for a higher furnace temperature of 720 °C. Moreover, the relative increase in temperature of Specimen # 17 compared to that of Specimen # 18 is 20°C larger. Additionally, it must be remembered that the latter specimen experience a much longer exposure time to the laser beam and that in both cases the laser beam power was kept constant.

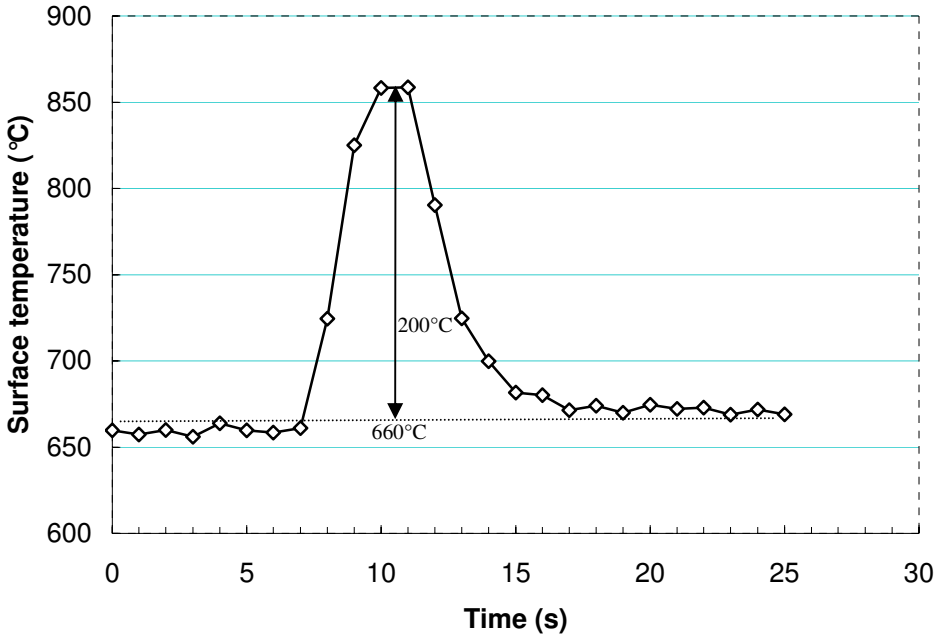


Figure 26. Surface temperature profile at one fixed location in Specimen # 17, laser power 55 W, Vs 17,8 mm/s, beam overlap 48%, Vt 1,2 mm/s, Tavg 660 °C.

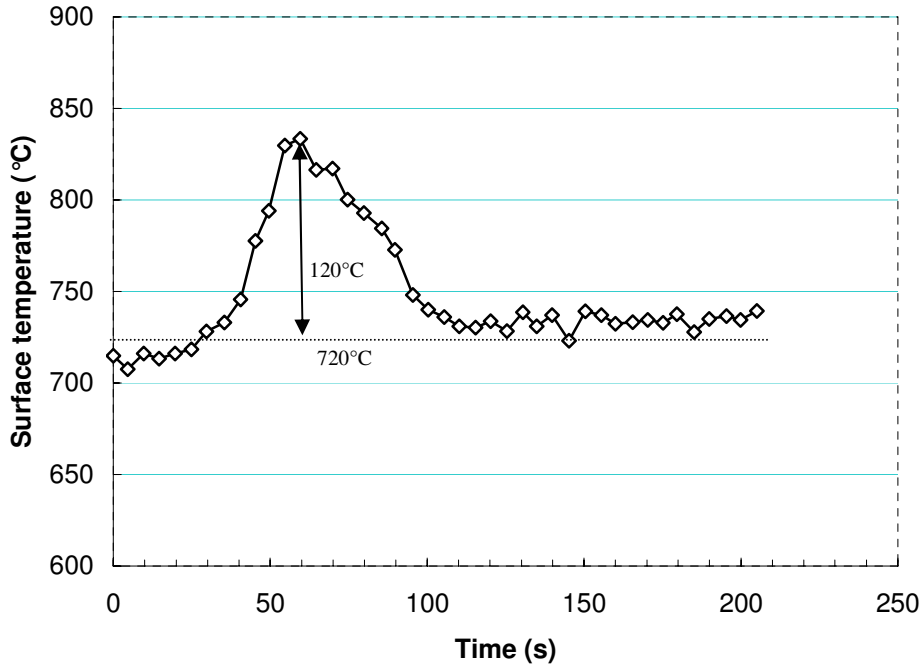


Figure 27. Surface temperature profile at a fixed location in Specimen #18 laser power 55 W, Vs 13,4 mm/s, beam overlap 95%, Vt 0,1 mm/s, Tavg 720 °C

## CONCLUSIONS

It has been shown that it is feasible to do DMLF of preplaced copper precursor powder using a raster scan low power $CO_2$ laser (66 watts before the F-theta lens) together with furnace temperature and inert gas atmosphere. Copper is known for its high surface reflectivity to infrared wavelengths, however, when in powder form its reflectivity apparently becomes smaller.

In one hand, powder beds of 0,5 mm depth, melted completely but showed an irregular shape due to a lack of powder quantity. On the other hand, due to the lack of laser power, it is not possible to melt the entire thickness of the 1 mm preplaced powder bed but only a surface layer of ~0,15 mm . However, this melt depth value is common to the multiple layer DMLF process. Full densification of the surface layer is achieved with a micro hardness HV value 20% lower than free oxygen copper. Overall mass density is almost a third of pure copper, due to the fact that below the molten surface a sintered layer has been produced with a 40% densification. Surface ripples are observed macroscopically, suggesting that surface tension gradient created surface waves in the liquid which then became frozen.

A counter intuitive behavior has possibly occurred and been observed. Specimens fabricated under higher average furnace temperature appeared not to have melted completely at the surface while others with lower furnace temperature had, when under same laser power level. Temperature history profiles measured suggest that a larger temperature increase is obtained for lower furnace temperatures than at higher ones. A simplified lumped heat balance model clearly shows that for low laser power, there is a critical furnace temperature, above which depth of melts is reduced drastically as this temperature approaches the melting temperature, unless laser power is increased. Larger surface heat losses by radiation than heat intake from the laser beam could explain this unusual observation. More empirical data is required to validate it.

A Cu-27wt%Ti alloy will be used a precursor material in the future, as it has an eutectic point at 820°C, almost 200°C lower than the melting point of pure Cu. This feature should increase the melt depth of such specimens.


### ACKNOWLEDGEMENTS

The authors of this work would like to acknowledge and express their gratitude to Fundación Andes in CHILE, for funding this research work under Grant Project C-13960/17.


### REFERENCES


1. C.R. Deckard, “Method and apparatus for producing part by selective sintering”, US Patent 4863538 (September 1989).

2. J.J.Beaman, J.W.Barlow, D.L.Bourell, and R.H.Crawford, Solid Freeform Fabrication: A New Direction in Manufacturing, (Kluwer Academic, 1997).

3. S. Das *et al.*, "Direct laser fabrication of a gas turbine engine component – microstructure and properties – part I", *SFF Symposium Proc,* 10, 1-9 (1998).

4. C. Atwood, M. Griffith, L. Harwell, E.Schlienger, Mark Ensz, J. Smugeresky, T. Romero, D. Green , D. Rechaway, "Laser Engineerd Net Shaping (LENS): a Tool for Direct Fabrication of Metal Parts", *SFF Symposium Proc,* 10, (1998).

5. L. Lü, J. Fuh and Y.S. Wong, Laser Induced Materials and Processes for Rapid Prototyping, (Kluwer Academic, 2001).

6. P. K. Venuvinod and W. Ma. Rapid prototyping : laser-based and other technologies, Kluwer Academic Publishers, (2004).

7. F. Erzincanh, M. Ermurat " Comparison of the direct metal laser fabrication technologies".
Gebze Institute of Technology. Dept. Design and Manufacturing Engineering, Gebze, Turkey. (Abril-2005) www.gyte.edu.tr/Akademik/Muh/imalat/0003.pdf

8. A. Simchi, F. Petzoldt, H. Pohl, "On the development of direct metal laser sintering for rapid tooling", J.Mat. Proc.Tech., 141, (2003) 319-328.

9. A. Simchi, H. Pohl, "Effects of laser sintering processing parameters on the microstructure and densification of iron powder", Materials and Engineering, A359 (2003) 119.128.

10. Y.Tang, H. Loh, Y. Wong, J. Fuh, "Direct laser sintering of a copper-based alloy for creating three-dimensional metal parts" Journal of Materials Processing Technology, 140 (2003), 368-372.

11. H.H. Zhu, L.Lu, J.Y.H. Fuh, "Development and characterization of direct laser sintering Cu-based metal powder", J.mat. Proc. Tech., 140 (2003) 314-317.

12. H.H. Zhu, L.Lu, J.Y.H. Fuh, C.C. Wu, "Effect of braze flux on direct laser sintering Cu-based metal powder", Materials & Desing, xxx (2004) xxx-xxx, article in press.

13. R. Morgan, C.J. Sutcliffe, W.O. Oneill, "Density analysis of direct metal laser re-melted 316L stainless steel cubic primitives", Journal of Materials Science 39, 2004, 1195-1205.

14. Y.Ning, Y.S. Wong, J.Y.H. Fuh, H.T. Loh, "An Approach to Minimize Build Errors in direct Metal Laser Sintering" IEEE Transactions on Automation Science and Engineering Vol. 3, No 1, January 2006.

15. C. Nickel, D. Barnett, G. Link, F. Prinz, "Residual stresses in Layered Manufacturing", *SFF Symposium Proc,* 11, 239-246, (1999).

16. X. Wu, J. Mei, "Near net shape manufacturing of components using direct laser fabrication technology", J. Mat. Proc. Tech, 135, (2003) 266-270.

17. H. Kyogoku, J.A. Ramos, D.L. Bourell, "Laser Melting of Ti-Ni Shape Memory Alloy", Proc. SFF Symposium 14, 668-675 (2003).

18 J. Ramos, D. Bourell, "Solidification Morphology Analysis of Selective Laser Melting of Cu Powder", Proceeding 15th Solid Free Form Fabrication Symposium, August, Austin Texas, 2004.

19. D. Bourell, M. Wohlert, N. Harlan, S. Das, J. Beaman, "Powder Densification Maps in Selective Laser Sintering", Advanced Engineering Materials, 4, N°9, (2002) 663-669.

20. R.M. German, Powder Metallurgy Science, (Metal Powder Industries Federation, Princeton, New Jersey 1984).

21. H.H Zhu, J.Y.H. Fuh, L.Lu, "Formation of Fe-Cu metal parts using direct laser sintering", Proc. Instn. Mech. Engrs. Vol 217, Part C: J. Mechanical Engineering Science, (2003) 139-146.

22. T.R. Anthony, H.E. Cline, "Surface rippling induced by surface tension gradients during laser surface melting and alloying", J. App.Phys. Vol. 48, N° 9, (1977) 3888-3894.

23. J. Ramos, "Surface Modification of Ceramic and Metallic Alloy Substrates by Laser Raster-Scanning", Ph.D. Thesis, The University of Texas at Austin, 2003.

24. M.Rombouts, L. Froyen, D. Bourell, J.P. Kruth, "Roughness after laser melting of iron based powders", Virtual modelling and rapid manufacturing – Bártolo (Eds), 2005 Taylor & Francis Group.

25. Kikuo Ujihara , Reflectivity of Metals at High Temperatures, Journal of Applied Physics , May 1972, Vol. 43, Issue 5, pp. 2376-2383.

26. http://www.webmat.com (August 2006)

27. International Copper Association, Ltd. Charts Prepared by: C.A. Thomson, W.M. Manganaro an F.R. Fickett, National Institute of Standards and Technology, Boulder, Colorado.